A Spatio-Temporal Threat and Dynamic Vulnerability-Based Risk Assessment for Electric Grids Facing Natural Disasters

Nayeemur Rahman[1], Md Asif Chowdhury[1], Sukumar Kamalasadan[1], and Sumit Paudyal[2]
[1]*The University of North Carolina at Charlotte, Charlotte, NC, USA*
[2]*Florida International University, Miami, FL, USA*
Email: {nrahman2, mchowd11, skamalas}@charlotte.edu, and spaudyal@fiu.edu

***Abstract*—Increasing extreme-weather threats—particularly hurricanes—require real-time, high-fidelity risk assessment to support resilient grid operations. This paper presents a structure-aware, data-driven online risk assessment framework that integrates dynamic system vulnerability with geographically varying threat likelihood via statistical inference. The framework combines Monte Carlo–based hurricane threat impact modeling with bus-level dynamic vulnerability indices derived from voltage, frequency, and generator rotor-angle responses to disturbance scenarios. The combination is based on a statistical inference correlation. The vulnerability and threat indices are then embedded using a probability-based weight selection to represent the overall risk in a normalized form that captures both the electric lines' threat attenuation and node-level similarity based on dynamic behavior. The framework is validated on the IEEE 39-bus system with inverter-based resources (IBRs) and subsequently scaled to a real-world 500-bus transmission grid. Results show that the proposed approach correlates strongly with traditional risk metrics while additionally capturing structural propagation effects. The proposed method offers actionable situational awareness for grid operators and is scalable for integration into online security assessment tools for future IBR-rich power systems.**

***Index Terms*—Integrated risk index, dynamic vulnerability assessment, hurricane threat analysis**

I. Introduction

Extreme weather events, such as hurricanes, ice storms, and wildfires, are increasingly challenging bulk power systems and exposing the limitations of traditional reliability-based planning methods [1]. These climate-driven events have become more common and severe with climate change, leading to more frequent and substantial large-scale outages [2]. The resulting impacts on transmission and distribution networks highlight the necessity for resilience-focused methodologies that extend beyond the conventional N-1 security framework [3]. System security has become the greatest challenge to maintenance resiliency, and risk assessment is not a fully explored area in bulk power systems. Early deterministic security assessment tools were mainly developed to prevent violations in specific contingency situations and do not effectively account for uncertainties in threat probability, component vulnerability, or cascading interactions [4], [5]. Consequently, power system operators and planners are increasingly adopting probabilistic and risk-based approaches that explicitly consider uncertainty in operational decision-making [6].

This work is supported by the U.S. Department of Energy's Office of Energy Efficiency and Renewable Energy (EERE) under the Solar Energy Technologies Office Award Number DE-EE0011369 (awarded to Sukumar Kamalasadan). Corresponding Author: S. Kamalasadan (email: skamalas@charlotte.edu).

979-8-3315-8138-1

A probabilistic risk-based security assessment (PRBSA) framework proposed in [7] extends the traditional risk concept to include threats, vulnerabilities, contingencies, and impacts. Recent studies also detailed the importance of representing extreme events through hazard models coupled with fragility or vulnerability functions that convert hazard intensity into component failure probabilities [8]. Such probabilistic connections enable risk assessment across spatially correlated components, enhancing the accuracy of Monte Carlo-based simulations and prioritizing high-risk assets in preventive planning [9]. Furthermore, recent advances in data-driven dynamic security assessment, including deep learning and physics-informed models, have improved short-term voltage stability and transient prediction under uncertainty [10]. The analytical basis for risk and resilience models is rooted in classical reliability theory and dynamic stability analysis, which quantify system robustness against random disturbances [11]. Dynamic stability, governed by generator swing equations and control loop interactions, is crucial to risk quantification, as transient responses in voltage, frequency, and rotor angle determine the system's ability to maintain synchronism under disturbances [12]. In modern grids dominated by IBRs, these dynamic responses are further affected by control frameworks, grid strength, and the spatial distribution of renewable energy generation.

Building on this foundation, this paper develops a structure-aware, probabilistic risk assessment framework that couples hurricane-driven threat exposure with dynamic, impact-weighted vulnerability estimation. The key contributions of the proposed framework are summarized as follows: (i) a spatio-temporal hurricane threat model that calculates bus-level exposure probabilities using wind-field physics and probabilistic fragility; (ii) a unified dynamic vulnerability metric that combines voltage, frequency, and phase responses from time-domain simulations, avoiding reliance on fixed heuristic weights; (iii) an impact-aware risk formulation that explicitly considers operational criticality through consequence weighting; (iv) scalability to large-scale transmission networks while maintaining the physical topology and spatial correlation of hazards.

The remainder of this paper is organized as follows. Section II formulates the problem and methodology. Section III reports the results and discussion. Section IV concludes the paper and outlines future research directions.

II. Problem Formulation and Methodology

We consider a transmission network, denoted as $\mathcal{G} = (\mathcal{V}, \mathcal{E})$, consisting of buses $i \in \mathcal{V}$ and energized lines $(i, j) \in \mathcal{E}$.

Each bus is associated with a hurricane-induced threat index $T_i \in [0, 1]$, which quantifies its proneness to hurricane impacts, while each line connects these buses and is characterized by a corresponding threat value, $T_{ij} \in [0, 1]$. These threat values are generated by a Monte Carlo hurricane model that employs the Holland wind profile formulation, along with spatio-temporal decay functions and logistic fragility relationships. To evaluate the dynamic resilience of each bus, we derive dynamic vulnerability indices, $v_i \in [0, 1]$ via time-domain analyses of short credible disturbances such as temporary faults and generator trips. The overall goal of this study is to compute (i) risk-coherent regions that demonstrate both structural and dynamic similarities among network components, and (ii) bus-wise integrated risk index (IRI) to effectively assess and mitigate the obtained risk.

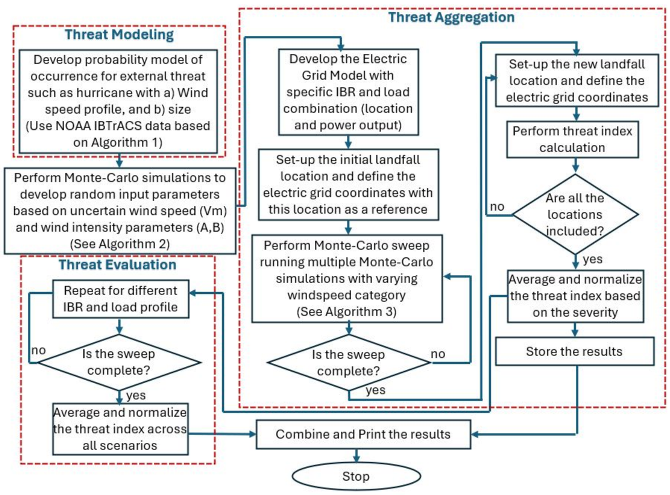

Fig. 1. Detail flowchart for the proposed Threat model

A. Threat Modeling

The probability of a particular threat (e.g., windstorm, earthquake, lightning) to any network topology is modeled based on three key dimensions: stress variable (s), spatial dependence (x,y), and time (t). Therefore, the methodology for threat modeling adopts a spatio-temporal probabilistic framework that characterizes the intensity of wind fields, spatial decay patterns, temporal exposure, and component fragility. Fig. 1 illustrates the detailed workflow for the hurricane threat modeling. The probability of threat (T_i) experienced at bus i, and the radial wind speed $V(r)$ at a distance r from the hurricane eye, which is modeled using the Holland formulation [13], are mathematically expressed as:

$$P_T(i) = P_{evd}(s) \cdot P_{\text{spatial}}(x_i, y_i) \cdot P_V(V) \cdot P_t(t_{\exp}), \quad (1)$$

$$V(r) = \left[\frac{AB\,(p_n - p_c)\,\exp\!\left(-\frac{A}{r^B}\right)}{\rho\, r^B} + \frac{r^2 f^2}{4} \right]^{1/2} - \frac{rf}{2} \quad (2)$$

where $P_{evd}(s)$ represents the probability density of the wind-speed stress variable derived from an extreme value distribution; $P_{\text{spatial}}(x_i, y_i)$ describes the spatial decay of hurricane intensity at specific bus coordinates (x_i, y_i); $P_V(V)$ denotes the conditional probability of component failure, given a wind speed V obtained from a logistic fragility model; and $P_t(t_{\exp})$ captures the temporal probability of exposure based on the storm residence time.

From the hurricane wind speed profile, we can get the probability density function of the stress variable (wind speed) through extreme value distribution (EVD) as:

$$P_{\text{evd}} = \frac{1}{\beta} e^{-\left(\frac{x-\mu}{\beta}\right)} e^{-e^{-\left(\frac{x-\mu}{\beta}\right)}} \quad (3)$$

where μ is the Mean value of wind speed for varying locations, and β is the Standard deviation of wind speed for varying locations.

The spatial distribution of hazard intensity is modeled using a two-dimensional Gaussian function, which provides a probabilistic representation of storm intensity across a geographic area [14]. The mathematical representation is given by:

$$P_{\text{spatial}}(x, y) = (A_F - b_0) \exp\left[-\frac{(x - x_c)^2}{s_1} - \frac{(y - y_c)^2}{s_2} \right] + b_0, \quad (4)$$

The exposure time ($t_{\exp}$), sampled based on storm category,is mathematically expressed as:

$$t_{\exp} \sim \mathcal{N}(\mu_{\text{cat}}, \sigma_{\text{cat}}), \quad (5)$$

Here, μ_{cat} and σ_{cat} are the mean and standard deviation of exposure times, respectively. The temporal occurrence probability can be represented as:

$$P_t(t_{\exp}) = 1 - e^{(-\lambda t_{\exp})} \quad (6)$$

where λ represents the hazard rate, governing the exponential decay of the exposure probability over time.

To assess the vulnerability of components susceptible to wind damage, a logistic fragility function is employed, determining the probability of failure as a function of the wind speed V:

$$P_V(V) = \frac{1}{1 + \exp[-\beta_1(V - \beta_0)]} \quad (7)$$

Here, β_0 indicates the wind speed threshold at which half of the components are expected to fail, and β_1 represents the sensitivity of the failure probability to changes in wind speed [15].

To quantify the threat posed to each bus, a normalized threat index $T_i \in [0, 1]$ is calculated. This normalization process ensures that threats are comparable across all buses. Implementing a Monte Carlo simulation across various locations, such as hurricane centers, storm intensities, and seasonal parameters, enables a comprehensive estimation of the expected threat distribution, which is crucial for subsequent vulnerability and risk analysis.

B. Dynamic Vulnerability Assessment

The assessment of dynamic vulnerability is performed through time-domain simulations that analyze line faults and generator trip scenarios. Three primary indicators are utilized to evaluate vulnerability, i,e, Voltage vulnerability, Frequency vulnerability, and rotor-angle vulnerability. The detailed flowchart for the workflow of the designed dynamic vulnerability model is illustrated in Fig. 2.

Voltage vulnerability is defined as follows:

$$\text{DUV}_i = \int \max(0, V_{\min} - V_i(t))dt \quad (8)$$

$$\text{DOV}_i = \int \max(0, V_i(t) - V_{\max})dt \quad (9)$$

979-8-3315-8138-1

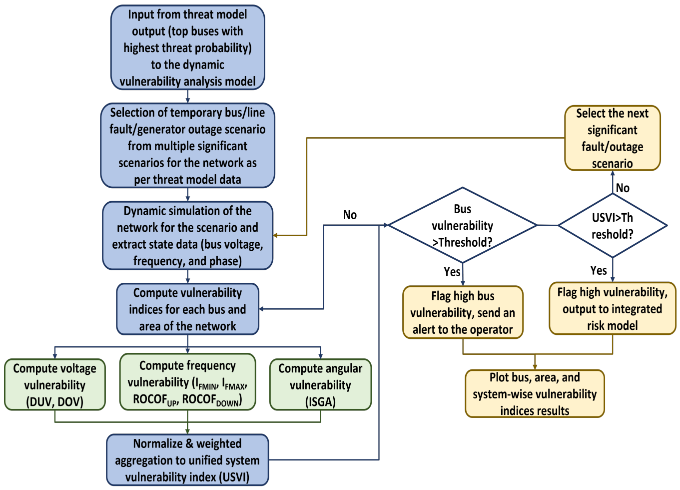

Fig. 2. Detail flowchart for the proposed dynamic vulnerability model

Here, $V_{\min} = 0.95$ p.u. and $V_{\max} = 1.05$ p.u. are the voltage thresholds, capturing under-voltage and over-voltage, respectively.

Frequency vulnerability is quantified using moving-average frequency deviation and Rate of Change of Frequency (RoCoF) metrics with a 0.5 s window and deadband. The indicator aggregates extreme deviations and RoCoF excursions using normalized threshold-based scoring [14].

Rotor-angle vulnerability indicator is calculated as follows:

$$\mathrm{ISGA} = \frac{1}{M_{\mathrm{tot}} T} \sum_{g=1}^{N_g} M_g \int_0^T \left(\delta_g(t) - \delta_{\mathrm{COA}}(t)\right)^2 dt. \tag{10}$$

where M_{tot} is the total inertia of the generators in the system, and $\delta_g(t)$ and $\delta_{\mathrm{COA}}(t)$ represent the rotor angles of generator g and the center of angle respectively over time T.

For each indicator type $k \in \{V, F, A\}$, where voltage, frequency, and angle indices are denoted as V, F, and A respectively, and bus $i \in \mathcal{V}$, The min–max normalized vulnerability index is defined as

$$\mathrm{normI}_{k,i} = \frac{I_{k,i} - I_k^{\min}}{I_k^{\max} - I_k^{\min}}, \tag{11}$$

where

$$I_k^{\min} = \min_{j \in \mathcal{V}} I_{k,j}, \qquad I_k^{\max} = \max_{j \in \mathcal{V}} I_{k,j}, \tag{12}$$

For each bus i, the normalized indicators for voltage, frequency, and generator angle are used to define adaptive self-weighted coefficients, which vary across each bus of the network based on the normalized indicator values:

$$w_{k,i} = \frac{\mathrm{normk}_i}{\sum \mathrm{normk}_j}, k \in \{V, F, A\}, j \in \mathcal{V}; \tag{13}$$

The Unified System Vulnerability Index (USVI) at bus i is then computed as:

$$\mathrm{USVI}_i = w_{V,i}\, \mathrm{normV}_i + w_{F,i}\, \mathrm{normF}_i + w_{A,i}\, \mathrm{normA}_i. \tag{14}$$

C. Integrated Threat and Vulnerability Assessment

In this work, the normalized threat index $T_i \in [0, 1]$ at bus i is interpreted as the probability of being exposed to damaging hurricane conditions, i.e., $P_T(i) \equiv T_i$. The unified vulnerability index $\mathrm{USVI}_i \in [0, 1]$ represents the severity that bus i (or its associated components) experiences given that a disturbance occurs in its vicinity.

An additional probability metrics $P_I(i) \in [0, 1]$ is introduced to represent the impact factor or severity weight of losing bus i. Following classical risk formulations, impact is modeled as a normalized consequence measure that reflects the criticality of the load and assets connected at each bus [11].

For each bus i, a consequence score $C_i \geq 0$ is defined as

$$C_i = \gamma_i\, P_i^{\mathrm{avg}}, \tag{15}$$

where P_i^{avg} is the average power flow, in pu, through bus i in the base operating condition and γ_i is a criticality weight (e.g., $\gamma_i = 1$ for standard nodes and $\gamma_i > 1$ for critical nodes like high load, generator, and IBR connected nodes). The bus-wise impact factor is then obtained by normalization:

$$P_I(i) = \frac{C_i}{\max_{j \in \mathcal{V}} C_j}, \tag{16}$$

so that $P_I(i) \in [0, 1]$, and the most critical bus will attain $P_I(i) = 1$.

D. Probabilistic Risk Formulation

In accordance with classical risk theory, system risk is defined as the joint effect of threat likelihood, conditional vulnerability, and the severity of consequences. In this study, the risk at each bus i, denoted as IRI_i, is modeled as a probabilistic product of three statistically independent but physically interconnected components:

$$\mathrm{IRI}_i = P_T(i) \cdot \mathrm{USVI}_i \cdot P_I(i). \tag{17}$$

This formulation ensures that risk increases only when (i) a hazard is likely to occur, (ii) the system response is dynamically severe, and (iii) the affected bus plays a critical operational role in the network.

III. Case Studies and Simulation Results

We conduct an extensive evaluation of our proposed framework using the IEEE 39-bus New England system [16]. Our analysis of disturbances incorporates a variety of scenarios, such as temporary faults on lines and buses, as well as the unexpected tripping of generators. Three synchronous generators located at bus-37, bus-31, and bus-36 are replaced with three IBRs with varying PV characteristics, which are situated in the north, west, and east sides of the system, respectively. To simulate the impact of hurricane events, we generate threat fields through 1000 Monte Carlo simulations, which model potential hurricane scenarios across all the nodes in the network. Table. I illustrates two sample test cases for the monte carlo threat model where two hurricane tracks were simulated, where the center was located at bus 11, and bus 2 respectively. The corresponding normalized threat index values can be seen in the table, which shows that the buses within the radius of maximum wind speed of the hurricane are the most probable locations to be affected.

The composite hurricane threat levels and their spatial distribution across the IEEE 39-bus system are illustrated in Fig. 3a, and 3b, where the threat index values are mostly high in the West and North area of the network.

The composite vulnerability assessment results, by aggregating all the high threat cases simulated from the hurricane threat composite model, has been illustrated in Fig. 4, which indicate

TABLE I
TOP-5 BUSES BY MONTE CARLO THREAT FOR TWO HURRICANE TRACKS AND COMPOSITE THREAT INDEX

Rank	Track: Center at Bus 11		Track: Center at Bus 2		Composite Threat	
	Bus #	Value	Bus #	Value	Bus #	Value
1	12	1.0000	30	1.0000	2	0.792
2	11	0.9986	37	0.9969	30	0.786
3	10	0.9979	2	0.9926	3	0.775
4	32	0.9961	25	0.9801	18	0.731
5	13	0.9928	3	0.8702	1	0.730

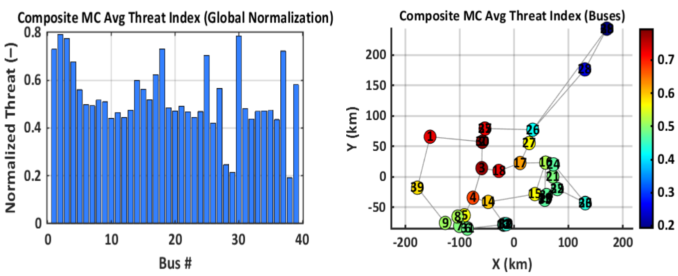

(a) (b)

Fig. 3. (a) Normalized composite threat index values and (b) their spatial distribution in the IEEE 39-bus network.

weak points in the network (bus-29, bus-28), emphasizing the need for targeted mitigation strategies. From Fig. 3 and Fig. 4, it can be seen that the buses exposed to higher hurricane intensities do not always coincide with the most vulnerable buses; dynamic voltage, frequency, and angle responses (and IBR locations) can shift vulnerability peaks.

Table II shows the top 6 buses with the highest threat, vulnerability, and risk index values, and Fig. 5 shows the bus-wise composite IRI plot for the 39 bus network. From the values, it can be seen that the risk index does not entirely depend on the threat and vulnerability model output, as the impact probability at each node significantly affects the IRI outcome. Consequently, the buses with a generator and IBR (bus 31, 37) have higher risk index values compared to other non-generator buses.

Further, we conducted a comprehensive evaluation of the proposed online risk–assessment model on a realistic 500-bus transmission system in South Carolina [17]. Our workflow was designed to closely replicate the methodologies established in the IEEE-39 study, but scaled up to account for the more complex geographic layout and the distribution of all substations and transmission lines across the state. Fig. 6 summarizes the Monte-Carlo hurricane threat outputs across all 500 bus

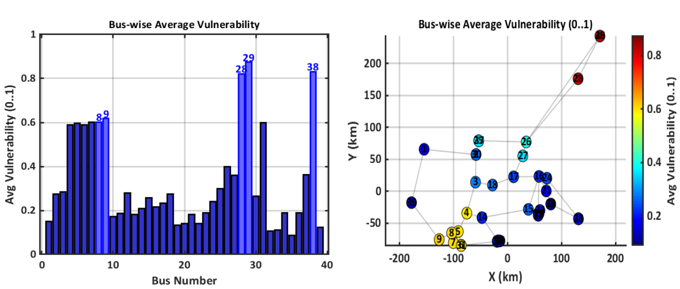

(a) (b)

Fig. 4. (a) Normalized composite vulnerability index values for all the buses and (b) their spatial distribution in the IEEE39 bus network.

TABLE II
TOP-6 BUSES BY NORMALIZED COMPOSITE THREAT, VULNERABILITY, AND RISK FOR THE IEEE 39-BUS

Rank	Threat		Vulnerability		IRI	
	Bus #	Value	Bus #	Value	Bus #	Value
1	2	0.792	29	0.874	31	1.000
2	30	0.786	38	0.831	37	0.895
3	3	0.775	28	0.820	6	0.555
4	18	0.731	9	0.618	5	0.499
5	1	0.730	8	0.602	7	0.459
6	37	0.722	7	0.601	29	0.408

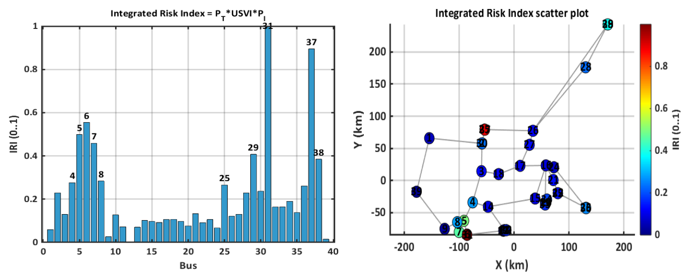

(a) (b)

Fig. 5. (a) Normalized composite integrated risk index values for all the buses and (b) their spatial distribution in the IEEE39 bus network.

locations. The left panel shows the normalized composite bus threat $\tilde{T}_i \in [0, 1]$ across all 500 buses; the right panel maps $\tilde{T}_i$ onto the geographic layout, revealing contiguous hazard corridors predominantly along the eastern coast of the network.

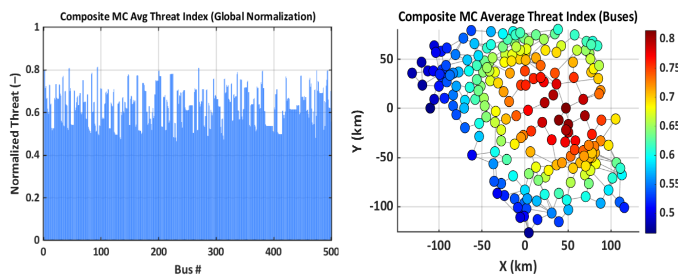

(a) (b)

Fig. 6. (a) Normalized composite threat index values and (b) their spatial distribution in the South Carolina 500 bus network.

In addition, Fig. 7 reports the bus-wise composite vulnerability, obtained by aggregating normalized voltage, frequency, and generator rotor angle vulnerability indices from temporary fault and generator trip cases. These incidents are correlated with the scenarios with the highest threat index values identified in the earlier simulations. The analysis reveals that vulnerability peaks are concentrated at specific buses within the network, indicating localized sensitivity to the assessed disturbance conditions used in our dynamic study. The top-6 buses by threat, vulnerability, and risk are listed in Table III.Bus 144 shows the highest risk, as it also has the highest active generation capacity, thereby a high impact probability in that node. Partial overlap (e.g., buses 44 and 45) in the threat and vulnerability index output indicates areas that are both exposed and dynamically susceptible. Fig.8 shows the per-bus difference for adaptive and fixed weightage vulnerability indices. The distribution is highly sparse: most buses exhibit nearly zero differences, while a small subset displays

979-8-3315-8138-1

TABLE III
TOP-6 BUSES BY NORMALIZED COMPOSITE THREAT, VULNERABILITY, AND RISK FOR THE SOUTH CAROLINA 500-BUS NETWORK.

Rank	Threat		Vulnerability		IRI	
	Bus #	Value	Bus #	Value	Bus #	Value
1	94	0.815	144	0.507	144	1.000
2	93	0.813	2	0.464	145	0.450
3	269	0.810	1	0.462	17	0.369
4	270	0.809	145	0.458	224	0.247
5	45	0.809	497	0.371	143	0.243
6	44	0.808	45	0.354	225	0.177

significant positive deviations, reaching up to approximately 0.27. This behavior indicates that the adaptive formulation does not inflate vulnerability uniformly; rather, it selectively increases scores for buses whose responses to disturbances are primarily driven by a single mechanism, such as voltage excursions, frequency deviations, or angle dispersions.

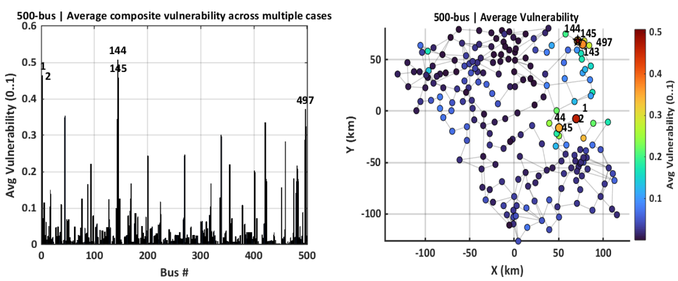

Fig. 7. (a) Normalized composite vulnerability index values and (b) their spatial distribution in the South Carolina 500 bus network.

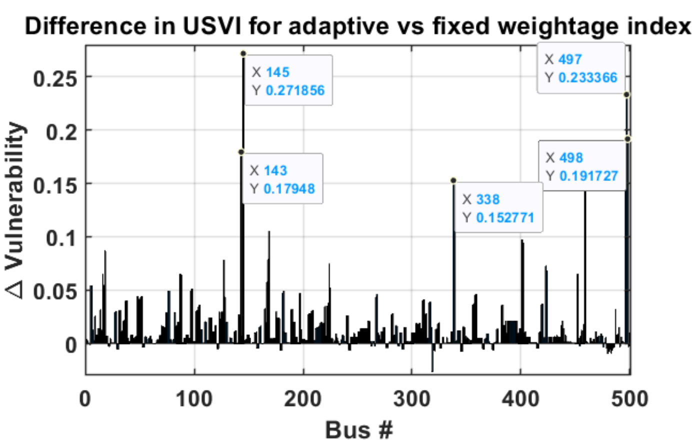

Fig. 8. Bus-wise difference in composite vulnerability index for the 500-bus system under the considered fault cases

IV. CONCLUSIONS

This work presents a structure-aware probabilistic risk assessment framework that integrates hurricane-driven threat fields, dynamic vulnerability indices, and consequence-weighted impact factors into a single metric called the Integrated Risk Index (IRI). The framework captures how hazards propagate across network corridors, how buses respond dynamically through variations in voltage, frequency, and rotor angle, and how the loss of each node affects the overall system based on its operational importance. Tests conducted on the IEEE 39-bus system and the 500-bus South Carolina network demonstrated that this framework effectively reorders risk along spatial hazard paths and inter-area boundaries. It highlights locations within the system where disturbances are most likely to trigger cascading effects or impacts that connect different regions. These findings emphasize the importance of combining physical topology, dynamic behavior, and exposure probability into a unified, data-driven metric for enhancing operational risk awareness.

V. ACKNOWLEDGMENT

The authors would like to thank and appreciate the help of Md Shamim Hasan, in developing the detailed model of the IEEE 39-bus system and IBR.

REFERENCES

[1] M. Panteli and P. Mancarella, "Influence of extreme weather and climate change on the resilience of power systems: Impacts and possible mitigation strategies," *Electric Power Systems Research*, vol. 127, pp. 259–270, 2015.
[2] Panteli, Mathaios and Mancarella, Pierluigi, "The grid: Stronger, bigger, smarter?: Presenting a conceptual framework of power system resilience," *IEEE Power and Energy Magazine*, vol. 13, no. 3, pp. 58–66, 2015.
[3] S. Espinoza, M. Panteli, P. Mancarella, and H. Rudnick, "Multi-phase assessment and adaptation of power systems resilience to natural hazards," *Electric Power Systems Research*, vol. 136, pp. 352–361, 2016.
[4] V. Vittal, "Online risk-based security assessment," *IEEE Transactions on Power Systems*, vol. 18, no. 1, pp. 258–265, 2003.
[5] R. Ramachandran, M. S. Hasan, and S. Kamalasadan, "Vulnerability assessment tool for large radial distribution system with high integration of distributed energy resources," in *2024 IEEE Industry Applications Society Annual Meeting (IAS)*. IEEE, 2024, pp. 1–7.
[6] E. Ciapessoni, D. Cirio, S. Grillo, S. Massucco, A. Pitto, and F. Silvestro, "An integrated platform for power system security assessment implementing probabilistic and deterministic methodologies," *IEEE Systems Journal*, vol. 7, no. 4, pp. 845–853, 2013.
[7] E. Ciapessoni, D. Cirio, G. H. Kjølle, S. Massucco, A. Pitto, and M. Sforna, "Probabilistic risk-based security assessment of power systems considering incumbent threats and uncertainties," *IEEE Transactions on Smart Grid*, vol. 7, no. 6, pp. 2890–2903, 2016.
[8] W. W. Kabre and M. R. Weimar, "Fragility functions resource report: Documented sources for electricity and water resilience valuation," Pacific Northwest National Laboratory (PNNL), Richland, WA (United States), Tech. Rep., 10 2022. [Online]. Available: https://www.osti.gov/biblio/1969999
[9] Q. Shi, C. Wang, W. Wei, and J. Wang, "Co-optimization of repairs and dynamic network reconfiguration for post-disaster distribution system resilience," *Applied Energy*, vol. 311, p. 118610, 2022.
[10] Z. Feng, X. Chen, Z. Lv, P. Sun, and K. Wu, "Transferable deep learning short-term voltage stability assessment with physics-informed topological feature engineering," *IEEE Open Journal of Power and Energy*, vol. 10, pp. 421–433, 2023.
[11] R. Billinton and R. N. Allan, *Reliability Evaluation of Power Systems*, 2nd ed. Boston, MA, USA: Springer, 1996.
[12] P. Kundur, *Power System Stability and Control*. New York, USA: McGraw-Hill Education, 1994.
[13] G. J. Holland, "An analytic model of the wind and pressure profiles in hurricanes," *Monthly Weather Review*, vol. 108, no. 8, 1980.
[14] E. Ciapessoni, D. Cirio, S. Massucco, A. Morini, A. Pitto, and F. Silvestro, "Risk-based dynamic security assessment for power system operation and operational planning," *Energies*, vol. 10, no. 4, 2017.
[15] S. Li, S. Wang, Q. Zhao, D. Liu, and C. K. Tse, "A risk assessment framework for large-scale synthetic power distribution networks considering historical hurricane disasters," *IEEE Transactions on Power Systems*, vol. 40, no. 5, pp. 3846–3858, 2025.
[16] T. Athay, R. Podmore, and S. Virmani, "A practical method for the direct analysis of transient stability," *IEEE Transactions on Power Apparatus and Systems*, vol. PAS-98, no. 2, pp. 573–584, 1979.
[17] A. B. Birchfield, T. Xu, K. M. Gegner, K. S. Shetye, and T. J. Overbye, "Grid structural characteristics as validation criteria for synthetic networks," *IEEE Transactions on Power Systems*, vol. 32, no. 4, pp. 3258–3265, 2017.

979-8-3315-8138-1